Sensorless Sliding-Mode Control of Induction Motors Using Operating Condition Dependent Models

Amuliu Bogdan Proca, *Student Member, IEEE,* Ali Keyhani, *Fellow, IEEE,* and John M. Miller, *Fellow, IEEE*

***Abstract*—A sensorless torque control system for induction motors is developed. The system allows for fast and precise torque tracking over a wide range of speed. The paper also presents the identification and parameter estimation of an induction motor model with parameters varying as functions of the operating conditions encountered in hybrid electric vehicles applications. An adaptive sliding mode speed-flux observer is developed and a cascade of discrete time sliding mode controllers is used for flux and current control. Simulation and experimental results prove the validity of the approach.**

***Index Terms*—Adaptive, induction motor, modeling, parameter estimation, sensorless control, sliding mode.**

I. Nomenclature

v_{ds}, v_{qs}	Stator voltage in stationary reference frame.
v^e_{ds}, v^e_{qs}	Stator voltage in synchronous reference frame.
i_{ds}, i_{qs}	Currents in stationary reference frame.
i^e_{ds}, i^e_{qs}	Currents in synchronous reference frame.
$I_s = \sqrt{i^{e2}_{ds} + i^{e2}_{qs}}$	Stator current.
λ_{dr}, λ_{qr}	Rotor fluxes in stationary reference frame.
λ_r	Rotor flux in synchronous reference frame.
n_p	Number of poles pairs.
ω_e, ω_r	Synchronous frequency and mechanical speed.
$\omega_s = \omega_e - n_p\omega_r$	Slip frequency (rotor current frequency).
$s = \omega_s/\omega_e$	Slip.
L_m, L_l	Magnetizing and leakage inductance.
R_s, R_r	Stator, rotor resistance.
T_e	Electromagnetic torque.
T	Stator temperature.
$\hat{}$, $*$	Estimated, reference values.

II. Introduction

In high performance applications, the induction motor is controlled through field orientation techniques that require knowledge of the rotor speed. Since speed sensors decrease the reliability of a drive system (and increase its price), a common trend in motor control is to use an observer to estimate speed.

There are five major speed estimation techniques in literature. Direct calculation methods [2]–[4] use motor equations to directly compute speed and are therefore prone to numerical errors and steady state errors. MRA observers [5]–[8] define two models (usually stator and rotor) that yield the same output (flux, back-emf, reactive power, etc). One model is speed independent while the other model contains speed terms. The output error is driven to zero by the speed estimate. An extended Kalman filter (EKF) method is proposed in [9] for rotor speed identification. The authors append a fifth state (speed) to the motor equations and use an EKF to observe it. Signal injection methods [10]–[14] use high frequency signals and motor saliency to accurately detect speed over wide ranges. Sliding mode observers [1], [15]–[18] use the estimated speed to correct a flux-current observer; the correction is based on a sliding mode surface that combines the current error with flux estimation. All known speed estimators depend on the induction motor model. Accurate knowledge of the model parameter is critical for speed estimation especially in the low speed range.

Considerable research has been done for induction motor parameter estimation [19]. Offline methods [20]–[22] target the estimation of all motor parameters with high accuracy. Self-commissioning methods [23], [24] focus on algorithms that can be implemented directly on the motor controller and ran as an initialization routine. Offline testing is not needed. They usually yield less precise results than offline methods. Online parameter estimation [25], [26] usually focuses on one or two parameters only (rotor or stator resistance); its main purpose is the tracking of the parameters that change while the motor is operating. There is relatively little research conducted in modeling the induction machine as a function of operating conditions [20].

The goal of this research is the development of a sensorless torque control system for hybrid electric vehicle applications. Due to the dependency of the control system to parameter knowledge, modeling and parameter estimation over a wide range of operating conditions of induction motors is also developed. The parameters of the motor are mapped to the operating conditions and are continuously updated while the motor is operating.

III. HEV Requirements for Sensorless Operation

The propulsion system of a hybrid electric vehicle (HEV) comprises both an internal combustion engine (ICE) and an electric motor (EM) [28]. The most common type of HEV is the parallel type, in which the both ICE and EM are directly

Manuscript received March 13, 2001; revised February 7, 2002. This work was supported in part by the National Science Foundation under Grant ECS9722844 and in part by the Ford Motor Company and the Ohio State University Electromechanical and Mechatronics Laboratory.

A. B. Proca and A. Keyhani are with Department of Electrical Engineering, The Ohio State University, Columbus, OH 43210 USA.

J. M. Miller is with Ford Motor Company, Detroit, MI 48126 USA.

Digital Object Identifier 10.1109/TEC.2003.811717

connected to the wheels. This structure presents a relative advantage in control over other induction motor applications, such as servos. The advantage is that the induction motor will virtually operate only at speeds above the idle speed of the ICE (currently 300–600 r/min). The only situation in which the IM will need to operate at lower speed will be the transient from zero (stalled) to idle speed. Since it is desired that HEV-s operation continues even with sensor failure, it is important that sensorlesss control algorithms be developed (without the addition of extra hardware). All known speed sensorless techniques are sensitive to variation of parameters. The induction motor parameters vary with the operating conditions, as is the case with all electric motors. Furthermore, for a propulsion application, the operating conditions will vary continuously. Speed (and input frequency) will change with driving cycles, traffic conditions, etc. Temperature is influenced by loading but also by ambient, season, etc. and can have variations as high as from 100°C. Operating flux levels will change with loading demands in order to obtain maximum energy efficiency. The parameters of the induction motor model will change as the motor changes operating conditions, and these changes need to be accounted for in control.

IV. Development of Variable Frequency Models

Fig. 1 shows the induction motor model used in this research in stationary reference frame for q-axis (d-axis are similar). As noted in [19], the model is equivalent (without any loss of information) to the more common T—model in which the leakage inductance is separated in stator and rotor leakage.

The following basic equations of induction machine can be derived:

$$\frac{d\lambda_{qr}}{dt} = n_p\omega_r\lambda_{dr} - \eta\lambda_{qr} + \eta L_m i_{qs} \tag{1}$$

$$\frac{d\lambda_{dr}}{dt} = -n_p\omega_r\lambda_{qr} - \eta\lambda_{dr} + \eta L_m i_{ds} \tag{2}$$

$$\frac{di_{qs}}{dt} = -\beta n_p\omega_r\lambda_{dr} + \eta\beta\lambda_{qr} - \gamma i_{qs} + \frac{1}{L_l}v_{qs} \tag{3}$$

$$\frac{di_{ds}}{dt} = \beta n_p\omega_r\lambda_{qr} + \eta\beta\lambda_{dr} - \gamma i_{ds} + \frac{1}{L_l}v_{ds} \tag{4}$$

with constants defined as follows:

$$\eta \equiv \frac{R_r}{L_m}, \quad \beta \equiv \frac{1}{L_l}, \quad \gamma \equiv \frac{R_s + R_r}{L_l}.$$

The electromagnetic torque expressed in terms of the state variables is

$$T_e = 3n_p\left(\lambda_{dr}i_{qs} - \lambda_{qr}i_{ds}\right). \tag{5}$$

The motor parameters were estimated offline. The motor was run at various operating conditions and small disturbance tests were applied. A speed sensor was used. The parameters were then estimated using a constrained optimization technique. Sensitivity analysis of the output to the parameters at different slip frequencies was employed to eliminate the parameters that yield low sensitivity. Outside rated conditions, the motor parameters change. Through a correlation analysis the authors isolated the parameter-operating condition dependency. Table I shows the motor parameters at rated conditions:

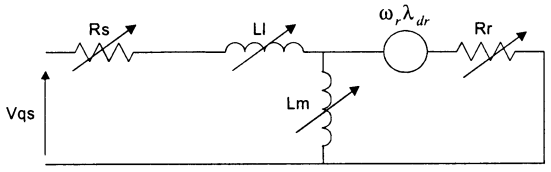

Fig. 1. Induction motor model in stationary reference frame(q-axis).

TABLE I
Induction Motor Rated Parameters

Rs	0.39 Ω
Ll	0.006 Henry
Lm	0.066 Henry
Rr	0.22 Ω

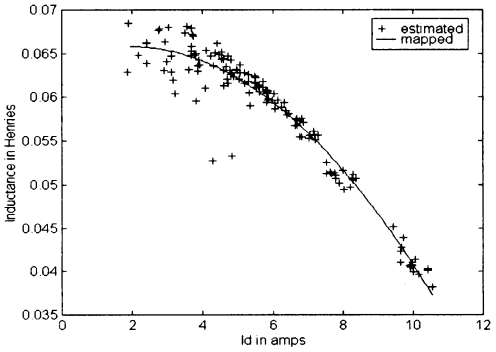

Fig. 2. L_m as function of i^e_{ds}.

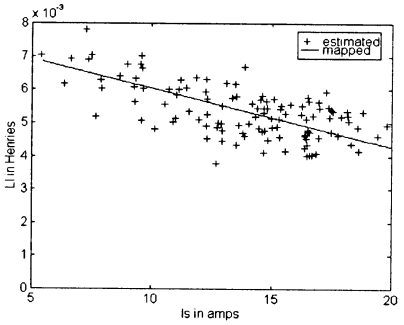

Fig. 3. L_l as function of I_S.

A strong correlation was observed between L_m and i^e_{ds} (L_m saturates with an increase in i^e_{ds}). A second order polynomial was used to represent the dependency (shown in Fig. 2)

$$L_m\left(i^e_{ds}\right) = k_1 \cdot i^{e^2}_{ds} + k_2 \cdot i^e_{ds} + k_3. \tag{6}$$

A strong correlation was also observed between L_l and I_S. L_l saturates with an increase in I_S. A linear approximation was used to represent the dependency (shown in Fig. 3)

$$L_l(I_s) = k_4 \cdot I_s + k_5. \tag{7}$$

The stator resistance was observed to be varying as a function of stator temperature. A linear approximation was used to represent the dependency (shown in Fig. 4)

$$R_s(T) = k_6 \cdot T + k_7. \tag{8}$$

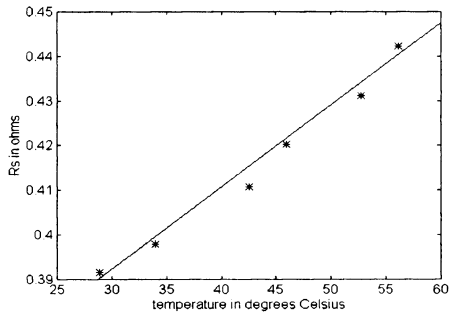

Fig. 4. R_S as a function of T.

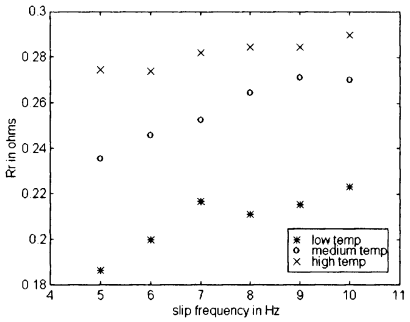

Fig. 5. R_r as a function of slip frequency.

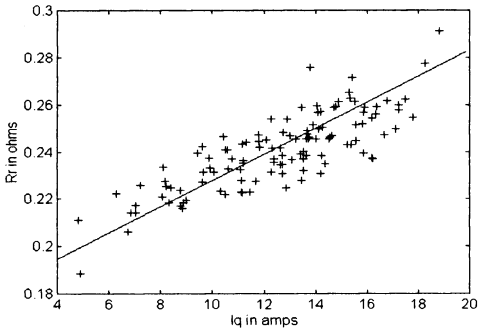

Fig. 6. R_r as a function of i_{qs}^e.

The rotor resistance varies as a function of two factors: slip frequency (through skin effect) and rotor temperature. Since rotor temperature is hardly measurable, the stator temperature was used instead. Fig. 5 shows the dependency of rotor resistance to slip at 3 temperature levels (measured on the stator) for locked rotor tests. Slip frequency is not measurable in a speed sensorless system. However, slip frequency is proportional to the i_{qs}^e current and therefore a correlation between R_r and i_{qs}^e exists; it was measured experimentally and is shown in Fig. 6. (stator temperature varied approximately 30 °C throughout the tests).

The authors used a linear approximation for the rotor resistance dependency on i_{qs}^e and stator temperature

$$R_r\left(i_{qs}^e\right) = k_8 \cdot i_{qs}^e + k_9 \cdot T + k_{10}. \tag{9}$$

Although more complicated (and more accurate) mappings can be derived, their implementation was impossible due to the time limitation of the DSP used for controlling the motor. The rotor resistance model is prone to errors due to the fact that stator temperature is used instead of rotor temperature and due to the choice of modeling (linear). However, due to the intrinsic robustness of the sliding mode observer, the effect of these errors on the speed estimation are relatively small at most operating conditions except for the low speed/high load region. The effects of rotor resistance estimation errors on speed estimation are shown in Section VII.

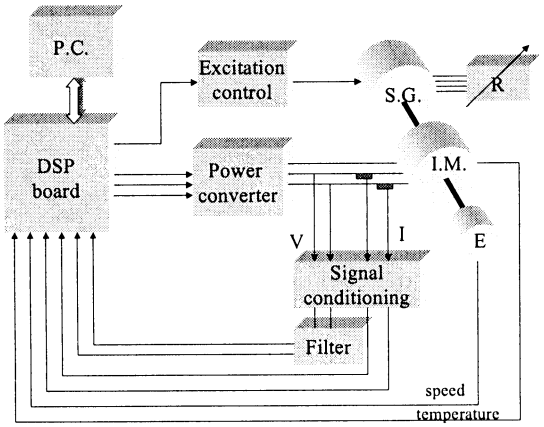

Fig. 7. Experimental setup.

V. Experimental Setup

The experimental setup used in this research is shown in Fig. 7. The induction motor (I.M.) is three-phase, four-pole, 5-Hp, 1750-r/min 220-V squirrel cage. The synchronous generator (S.G.) is two phase, two pole, 5 Hp 440 V and is used as a load. The 5-kW variable resistor box (R) loads the synchronous generator. A variable DC power supply controls the excitation of the synchronous generator. The motor is driven by a 400-V/30-A power converter capable of switching at 20 kHz. A dual processor (TMS320C31 Master and TMS320P14 Slave) DSP board used both for control and data acquisition. A 1024 pulse/revolution incremental optical encoder is used for speed measurement. The PWM cycle is 240 μs and the data acquisition sampling time is 60 μs. In order to avoid aliasing, the measured voltage is passed through a low pass filter prior to being acquired. The synchronous generator can be controlled simultaneously with the motor using the DSP board through the excitation voltage.

VI. Sensorless Torque Control Development

A simplified block diagram of the control diagram is shown in Fig. 8.

A. Adaptive Sliding Mode Observer

The speed-flux sliding mode observer equations are based on the induction motor current and flux equations

$$\frac{d\hat{i}_{qs}}{dt} = -\beta\hat{\omega}_r\hat{\lambda}_{dr} + \eta\beta\hat{\lambda}_{qr} - \gamma\hat{i}_{qs} + \frac{1}{L_l}v_{qs} \tag{10}$$

$$\frac{d\hat{i}_{ds}}{dt} = \beta\hat{\omega}_r\hat{\lambda}_{qr} + \eta\beta\hat{\lambda}_{dr} - \gamma\hat{i}_{ds} + \frac{1}{L_l}v_{ds} \tag{11}$$

$$\frac{d\hat{\lambda}_{qr}}{dt} = \hat{\omega}_r\hat{\lambda}_{dr} - \eta\hat{\lambda}_{qr} + \eta L_m\hat{i}_{qs} \tag{12}$$

$$\frac{d\hat{\lambda}_{dr}}{dt} = -\hat{\omega}_r\hat{\lambda}_{qr} - \eta\hat{\lambda}_{dr} + \eta L_m\hat{i}_{ds}. \tag{13}$$

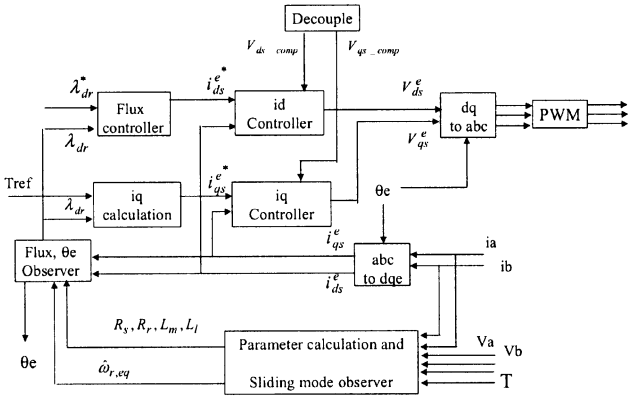

Fig. 8. Control structure.

Let a sliding surface be

$$s = (\hat{i}_{qs} - i_{qs})\hat{\lambda}_{dr} - (\hat{i}_{ds} - i_{ds})\hat{\lambda}_{qr} \tag{14}$$

and let

$$\hat{\omega}_r = \omega_0 \text{sign}(s). \tag{15}$$

By choosing a large enough $\hat{\omega}_0$, it can be shown that s can be driven to zero in a finite time[1], implying the current estimates $(\hat{i}_{ds}, \hat{i}_{qs})$ and flux estimates $\hat{\lambda}_{dr}$, $\hat{\lambda}_{qr}$ will converge to their real values in a finite time. $\hat{\omega}_r$ will contain high frequency components (due to its switching nature) and a low frequency component. The low frequency component is equal to the speed. The proof of convergence [1] will not be presented in this paper due to its length. Since $\hat{\omega}_r$ is a switching function, it cannot be used as such outside the observer ((10)–(13)). The smoothed value of $\hat{\omega}_r$ can be found by passing it through a low-pass filter

$$\hat{\omega}_{r,eq} = \frac{1}{1 + s \cdot \tau}\hat{\omega}_r. \tag{16}$$

The selection of the speed gain (ω_0) has two major constraints: the gain has to be large enough to insure that sliding mode can be enforced; a very large gain can yield to instability of the observer to discrete time integration. Through simulations, the authors used a linear function to tune the gain of the sliding mode observer to the equivalent speed

$$\omega_0 = \hat{\omega}_{r,eq} \cdot 0.3 + 60. \tag{17}$$

The presence of offsets in the measured signals can negatively influence the speed estimation. A dc offset in the measured input voltage "sees" only small impedance (just like in a dc test) and yields a large estimated current error. This, in turn, yields an oscillation in the estimated speed. In order to compensate the offsets, the authors used a recursive average value estimator for the measured voltages and currents

$$V_{\text{offset}}(k+1) = V_{\text{measured}}(k) \cdot \frac{1}{N} + V_{\text{offset}}(k) \cdot \frac{N-1}{N} \tag{18}$$

where N is the number of samples for averaging and should be larger than the number of samples for one period at lowest input frequency. Since at steady state the signals are sinusoidal, the mean average is equal to the measurement offset and must be subtracted from the measurements prior to using into the observer.

The sliding mode observer structure allows for the simultaneous observation of rotor fluxes. However, due to the limited sampling frequency, the numerical integration of the fourth order observer equations yields errors on flux observation, although the observer produces correct speed estimates. The integration error increases with supply frequency. Instead of using the flux-speed estimator for flux estimates, the authors used a second order observer

$$\frac{d\hat{\lambda}_{qr}}{dt} = \hat{\omega}_{r,eq}\hat{\lambda}_{dr} - \eta\hat{\lambda}_{qr} + \eta L_m i_{qs} \tag{19}$$

$$\frac{d\hat{\lambda}_{dr}}{dt} = -\hat{\omega}_{r,eq}\hat{\lambda}_{qr} - \eta\hat{\lambda}_{dr} + \eta L_m i_{ds}. \tag{20}$$

This observer produces correct flux estimates as shown in [1].

B. Alternative Speed Estimation for Speed Below 20 r/min

The sliding mode observer with parameters mapped to the operating conditions cannot correctly estimate speeds below 20 r/min (in simulation the estimator works down to approximately 1 r/min). There are two main causes to this problem. First, the speed component in the observer equations becomes very small compared to the other terms in the equations and any parameter mismatch or measurement error will yield large speed estimation errors. Second, in order to maintain a flux level below saturation, at low frequency the amplitude of supply voltage is very small (below 5 V for speed below 20 r/min). Since voltage transducers are designed for approximately 100 times this value, there is considerable amount of noise and measurement error. The authors used instead of the sliding mode speed observer an input frequency observer. The observer is based on a least square estimator. Let a sample of the d axis current (stationary reference) at instant n be

$$\begin{aligned} i_{ds}(n) =& I_s \sin(\omega t + \varphi) \\ =& I_s \sin(\omega(t - TS) + \varphi + \omega \cdot TS) \\ =& i_{ds}(n-1)\cos(\omega \cdot TS) + i_{qs}(n-1) \\ & \times \sin(\omega \cdot TS). \end{aligned} \tag{21}$$

Assuming that the input frequency does not change considerably over the estimation process (approximately 6 ms), the i_{ds} current can be written as

$$y_n = h_n \cdot \theta_n \tag{22}$$

where $y_n = i_{ds}(n)$, $h_n = [i_{ds}(n-1)\ i_{qs}(n-1)]$, $\theta_n = [\theta_n(1)\ \theta_n(2)] = [\cos(\omega TS)\ \sin(\omega TS)]$, and TS is the sampling time. The estimation process recursively calculates the parameter vector θ_n over 100 samples. The procedure can be summarized as

1) Initialize

$$P_1^{-1} = h_1' \cdot h_1. \tag{23}$$

2) Recursively estimate θ_{n+1} using least squares

$$P_n^{-1} = P_n^{-1} + h_n' \cdot h_n, \quad k_{w,n} = P_n \cdot h_n' \tag{24}$$

$$\theta_{n+1} = \theta_n + k_{w,n} \cdot (y_n - h_n \cdot \theta_n). \tag{25}$$

3) After 500 samples, calculate

$$\hat{\omega} = \frac{1}{TS} \sin^{-1} \left(\frac{\theta_n(2)}{\sqrt{\theta_n^2(2) + \theta_n^2(1)}} \right). \quad (26)$$

The frequency of the output is continuously monitored. When it falls below 1 Hz, the output of the sliding mode observer is not used anymore, and instead the supply frequency is used. Although perfect field orientation cannot be achieved (because slip frequency is neglected), the motor performed relatively well at very low speed (below 20 r/min).

C. Discrete Time Flux Control—Outer Loop

The rotor flux dynamics in synchronous reference frame are linear and only dependent on the d-current input. A discrete time controller is used. The flux controller equation is

$$i_{ds}^e(n) = \frac{\lambda_{dr}^{e^*} - a_\lambda \cdot i_{ds}^e(n)}{b_\lambda} \quad (27)$$

where $a_\lambda = e^{-\eta \cdot TS2}$, $b_\lambda = 1 - a_\lambda/\eta \cdot L_m$, $TS2$—sampling time of the flux controller.

The flux reference can either be left constant or modified to accomplish certain requirements (minimum current, maximum efficiency, field weakening). For speeds above rated, it is necessary to weaken the flux so that the supply voltage limits are not exceeded. The q-current reference is calculated from the torque equation to provide fast torque tracking

$$i_{qs}^{e^*} = \frac{T_{\text{ref}}}{3n_p \cdot \lambda_{dr}^e}. \quad (28)$$

D. Current Control-Inner Loop

By rewriting the discrete version of the current equations one obtains

$$i_{qs}^e(n+1) = a i_{qs}^e(n) + b V_{qs\_\text{comp}}(n) + b v_{qs}^e(n) \quad (29)$$
$$i_{ds}^e(n+1) = a i_{ds}^e(n) + b V_{ds\_\text{comp}}(n) + b v_{ds}^e(n) \quad (30)$$

where $a = e^{-\gamma \cdot TS}$, $b = 1 - a/\gamma \cdot \sigma \cdot L_S$, TS—sampling time

$$v_{qs\_\text{comp}} = -n_p \omega_r \lambda_r^e - \sigma L_s \omega_e i_{ds}^e \quad (31)$$
$$v_{ds\_\text{comp}} = \sigma L_s \left(\omega_e i_{qs}^e + \eta \cdot \beta \cdot \lambda_r^e \right). \quad (32)$$

The control signals can then be calculated so that the currents reach their references in one sampling period

$$v_{qs}^e(n) = \frac{i_{qs}^{e^*} - a \cdot i_{qs}^e(n)}{b} - V_{qs\_\text{comp}}(n) \quad (33)$$
$$v_{ds}^e(n) = \frac{i_{ds}^{e^*} - a \cdot i_{ds}^e(n)}{b} - V_{ds\_\text{comp}}(n). \quad (34)$$

Since the calculated value of the control may exceed the maximal possibilities of the converter (dc bus voltage), an equivalent control was used. For the d-axis, the control is

$$v_{ds\_eq}^e(n) = \begin{cases} v_{ds}^e(n), & \text{if } v_{ds}^e(n) \le U_{\max} \\ U_{\max} \cdot \text{sign}(v_{ds}^e(n)), & \text{if } v_{ds}^e(n) > U_{\max}. \end{cases} \quad (35)$$

The q-axis control is similar. The net advantage of such control is that it preserves the good dynamic performance of the continuous time sliding mode control while eliminating chattering. However, since the control does not have an error correcting term (like a PI controller has), any parameter mismatch, delay, quantization error, etc. will result in a steady state tracking error. The authors added a small error integrating term to the control to correct the problem

$$v_{ds\_\text{new}}^e(n) = v_{ds\_eq}^e(n) + k_i \cdot \left(i_{ds}^{e^*}(n) - i_{ds}^e(n) \right) + e_{\text{old}}(n)$$
$$e_{\text{old}}(n) = k_i \left[i_{ds}^{e^*}(n-1) - i_{ds}^e(n-1) \right] + e_{\text{old}}(n-1),$$
$$e_{\text{old}}(1) = 0. \quad (36)$$

TABLE II
SPEED ESTIMATION ERRORS (%) AS FUNCTION OF R_r ERROR

Speed, Load(i_{qs}^e)	Δ Rr=-75%	Δ Rr=-50%	Δ Rr=50%	Δ Rr=75%	Δ Rr=100%
100 rpm, 0.3 A	1.27	1.35	-1.01	-1.24	-1.56
100 rpm, 10 A	26.21	17.26	-17.95	-26.22	-35.64
100 rpm, 17 A	44.21	29.73	-30.21	-45.85	-60.25
500 rpm, 0.3 A	0.63	0.38	-0.41	-0.57	-0.69
500 rpm, 10 A	5.34	3.46	-3.75	-5.52	-7.38
500 rpm, 17 A	10.02	6.31	-6.62	-9.16	-12.13
1000 rpm, 0.3 A	0.49	0.41	-0.45	-0.53	-0.66
1000 rpm, 10 A	3.81	1.79	-1.86	-2.81	-3.75
1000 rpm, 17 A	4.82	3.17	-2.93	-4.43	-6.11

VII. SIMULATIONS AND EXPERIMENTAL RESULTS

A. Simulations

The effect of rotor resistance errors on speed estimation was analyzed since this parameter is prone to more inaccuracy than others. Errors up to 100% in rotor resistance values were considered. The analysis was conducted at three speed levels for which three loading levels (represented by i_{qs}^e) were considered. The results are shown in Table II. It can be seen that except for the low speed and high load range, errors in rotor resistance values have little impact on speed estimation.

The control scheme presented in Section VI was simulated using Simulink. For operation of the motor above 20 r/min, the control scheme performed very well. The following graphs show different simulation tests performed at various speeds. The bottom graph shows the torque reference tracking. Figs. 9 and 10 show that good tracking can be obtained in the entire range (except below 20 r/min). Fig. 11 shows a test performed at very low speed (below 20 r/min).

It can be observed that in the regions where speed fell below the threshold, speed estimates are constant for larger periods of time. This is due to the intrinsic delay of the least-square observer. Also, some oscillation can be seen around 20 r/min as the controller moves between sliding mode and least-square estimation of speed.

B. Experimental Results

1) Flux-Speed Convergence: The authors tested the speed-flux observer at various operating conditions. One test consisted in disturbing the initial conditions (currents and fluxes were made equal to zero at 1 s) and then observing if the observer recovers and converges (dotted line, Fig. 12). For comparison, the

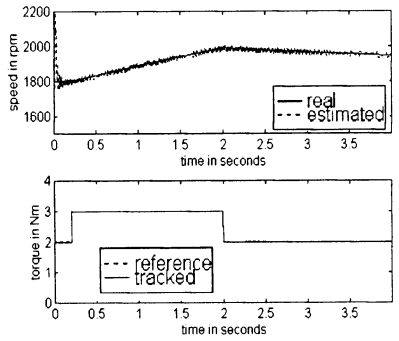

Fig. 9. Torque tracking in the 1500–2400-r/min range.

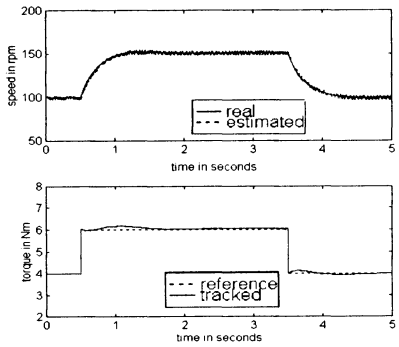

Fig. 10. Torque tracking in the 20–500-r/min range.

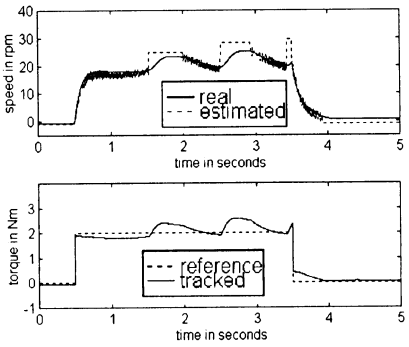

Fig. 11. Torque tracking in the 0–20–r/min range.

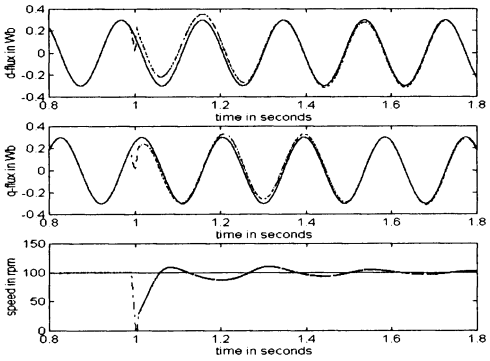

Fig. 12. Flux-speed observation with initial condition disturbance at 100 r/min.

flux estimates from the second order flux observer (with speed measurements) were used (solid line). Both speed and flux converge in a short time. Due to the limited space of this paper, only one test is shown.

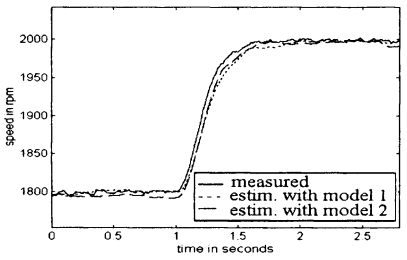

Fig. 13. Estimated speed in the 1500–2400–r/min range at medium flux, light load.

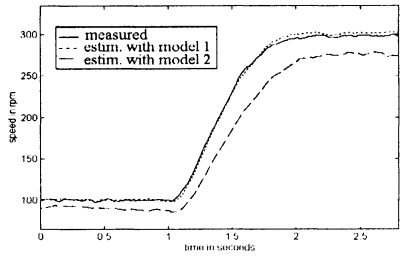

Fig. 14. Estimated speed in the 100–300–r/min range, at low flux, high load.

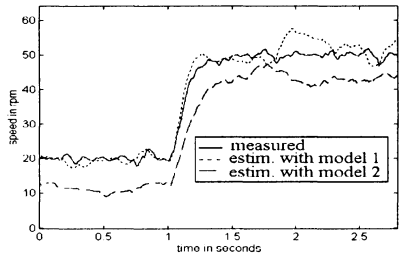

Fig. 15. Estimated speed in the 20–50–r/min range at high flux, low load.

2) Influence of Parameter Variation on Speed Estimation: The authors tested the sliding mode speed observer using rated parameters and varying (model-based) parameters. The flux and load levels were varied within their bounds. It was observed that except at rated conditions, the speed estimates for the model with rated (fixed) parameters exhibited considerable more error than for the model with varying parameters. It is a well-known fact that the temperature under the hood of vehicle can be as high as 80 °C. However, in the lab test, the temperature variation was relatively low (30 °C) during the lab tests; for in vehicle applications, larger temperature variation should be expected that will result in a larger difference in errors between the variable frequency models (model 1) and the rated parameter model (model 2). Figs. 13–15 present results of the tests (measured and observed speed). In order to quantify the observer performance, the mean and the rms error between measured and estimated speed was recursively calculated. The estimation errors for all speed ranges (maximal values) are summarized in Table III for the model with constant parameters and in Table IV for the proposed model. The mean, maximal, and standard deviation of the error are calculated at steady state. All relative values are in respect to the measured speed. As reported for other speed estimators, the relative value of the mean error decreases with a speed increase. While the

TABLE III
ESTIMATION ERROR FOR MODEL WITH RATED PARAMETERS

Speed	Mean Error		Standard deviation		Maximal Error	
(rpm)	Abs (rpm)	Relative (%)	Abs (rpm)	Relative (%)	Abs (rpm)	Relative (%)
20	7.73	38.63	3.19	15.97	10.27	51.34
50	6.90	13.80	2.18	4.35	9.31	18.61
100	9.52	9.52	1.45	1.45	12.60	12.60
200	25.57	12.79	7.99	4.00	39.37	19.68
500	21.50	4.30	6.81	1.36	33.63	6.73
1000	20.23	2.02	6.52	0.65	29.01	2.90
1200	16.96	1.41	1.80	0.15	19.72	1.64
1800	7.89	0.44	3.25	0.18	17.21	0.96
2000	11.76	0.59	3.64	0.18	18.45	0.92
2400	11.92	0.50	3.71	0.15	17.45	0.73

TABLE IV
ESTIMATION ERROR FOR PROPOSED MODEL

Speed	Mean Error		Standard deviation		Maximal Error	
(rpm)	Abs (rpm)	Relative (%)	Abs (rpm)	Relative (%)	Abs (rpm)	Relative (%)
0.5	1.91	382.00	1.82	364.00	4.1	820.00
5	3.64	72.80	2.49	49.80	8.96	179.20
10	3.24	32.40	1.38	13.80	3.97	39.70
15	3.14	20.93	1.01	6.73	4.78	31.87
20	2.36	11.78	2.69	13.47	6.03	30.14
50	4.03	8.07	2.27	4.55	6.11	12.22
100	8.23	8.23	3.26	3.26	13.75	13.75
200	7.16	3.58	5.96	2.98	13.44	6.72
500	6.82	1.36	4.42	0.88	12.50	2.50
1000	6.53	0.65	3.40	0.34	15.03	1.50
1200	8.15	0.68	2.62	0.22	10.66	0.89
1800	7.73	0.43	3.62	0.20	18.32	1.02
2000	9.70	0.48	3.71	0.19	19.10	0.96
2400	10.20	0.43	4.51	0.19	21.32	0.89

relative mean error at speed above 1000 r/min is small for both models, considerable difference can be observed below this speed. For speed below 20 r/min, both models performed poorly, justifying the use of a non-model-based speed estimator (results for this range are in Table IV).

3) Control Above 20 r/min: For operation of the motor above 20 r/min, the control scheme performed very well. Figs. 16 and 17 show tests performed at low speed. The top graph shows the measured (dotted line) versus estimated speed (solid line). The bottom graph shows the torque reference tracking. The observed torque is calculated using an observer that uses speed measurements. It can be seen that good tracking can be obtained in the entire range (except below 20 r/min).

4) Control Below 20 r/min: To qualify the situations in which the speed falls below the 20-r/min limit and which can produce large speed estimation errors, the authors used the frequency of the supply voltage as a measurement of speed. When it falls below 1 Hz, the output of the sliding mode observer is not used anymore, and instead the supply frequency is used. Fig. 18 shows an example of a test. Although speed observation is relatively poor, the system can still track torque.

Furthermore, the very low speed operation of the induction motor is relatively rare in propulsion system for automotive application so the overall performance of the motor-controller system will not be affected considerably.

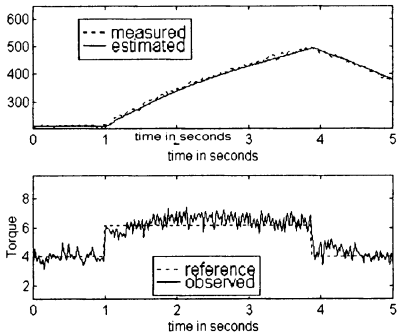

Fig. 16. Torque tracking in the 20–500–r/min range.

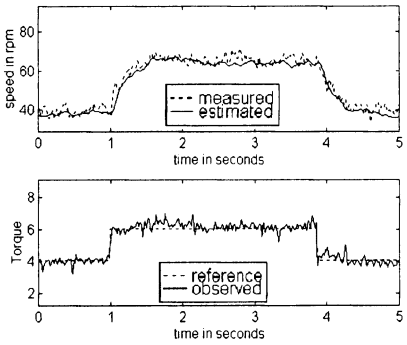

Fig. 17. Torque tracking in the 40–80–r/min range.

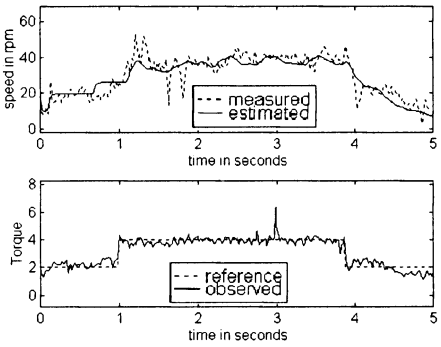

Fig. 18. Torque control in the 0–50-r/min range.

VIII. CONCLUSION

A sensorless torque control system for induction motors is developed in this research. The system allows for fast and precise torque tracking over a wide range of speed, from 20 to 2400 r/min. Both the speed observer and the control scheme are model based. The authors modeled the induction motor over a wide range of operating conditions, consisting of wide speed, load and flux ranges. By employing a sensitivity analysis of the output to each variable at various slip frequencies, the parameters that yielded low sensitivity were eliminated. Through a correlation study, the dependencies between parameters and the variables characterizing operating conditions were isolated. The parameters were then mapped to these variables. Although the procedure was developed offline, both parameter estimation and mapping to operating conditions can be automated for an industrial setting.

The speed estimator is an adaptive sliding mode observer. Gain adaptation of the observer is needed to stabilize the observer when integration errors are present. The design and implementation issues of the observer were analyzed (gain adap-

tation, offset cancellation, etc). The observer can accurately observe speed down to approximately 20 r/min. Below this level, due to the low levels of voltage (1% of full scale) and to possible parameter mismatches, the speed observations are inaccurate. The authors proposed an alternative method in which the input frequency is used as an observation of speed. The control algorithm is field oriented using discrete time sliding mode controllers for current and flux tracking. The discrete time sliding mode controller combines the fast response of any sliding mode controller while eliminating the chattering characteristic to continuos time sliding mode controllers. The controller was shown to perform very well except for the very low speed ranges. This poor performance at very low speed is due to the inaccurate speed observations at those speeds. However, the motor is able to respond with a speed increase when an increased torque command is received.

Also, once the very low speed range is passed, the high performance control resumes. This low speed behavior is acceptable for HEV applications, when motor speed falls below stall speed (of IC engine) only at start-up and shut down.

REFERENCES

[1] V. Utkin, J. Guldner, and J. Shi, *Sliding Mode Control in Electromechanical Systems*. New York: Taylor & Francis, 1999.

[2] T. Ohtani, N. Takada, and K. Tanaka, "Vector control of induction motor without shaft encoder," *IEEE Trans. Ind. Applicat.*, vol. 28, pp. 157–164, Jan./Feb. 1992.

[3] K. Akatsu and A. Kawamura, "Sensorless very low-speed and zero-speed estimations with online rotor resistance estimation of induction motor without signal injection," *IEEE Trans. Ind. Applicat.*, vol. 36, pp. 764–771, May/June 2000.

[4] E. G. Strangas, H. K. Khalil, B. A. Oliwi, L. Laubinger, and J. M. Miller, "Robust torque controller for induction motors without rotor position sensor: Analysis and experimental results," *IEEE Trans. Energy Conversion*, vol. 14, pp. 1448–1456, Dec. 1999.

[5] C. Schauder, "Adaptive speed identification for vector control of induction motors without rotational transducers," *IEEE Trans. Ind. Applicat.*, vol. 28, pp. 1054–1061, Sept./Oct. 1992.

[6] F. Z. Peng and T. Fukao, "Robust identification for speed-sensorless vector control of induction motors," *IEEE Trans. Ind. Applicat.*, vol. 30, pp. 1234–1240, Sept./Oct. 1994.

[7] J. Maes, J. Jehudi, and A. Melkebeek, "Speed-sensorless direct torque control of induction motors using an adaptive flux observer," *IEEE Trans. Ind. Applicat.*, vol. 36, pp. 778–785, May/June 2000.

[8] L. Zhen and L. Xu, "Sensorless field orientation control of induction machines based on a mutual MRAS scheme," *IEEE Trans. Ind. Electron.*, vol. 45, pp. 824–831, Oct. 1998.

[9] Y.-R. Kim, S.-K. Sul, and M.-H. Park, "Speed sensorless vector control of induction motor using extended kalman filter," *IEEE Trans. Ind. Applicat.*, vol. 30, pp. 1225–1233, Sept./Oct. 1994.

[10] P. L. Jansen and R. D. Lorenz, "Transducerless position and velocity estimation in induction and salient AC machines," *IEEE Trans. Ind. Applicat.*, vol. 31, pp. 240–247, Mar./Apr. 1995.

[11] D. Hurst, T. G. Habetler, G. Griva, F. Profumo, and P. L. Jansen, "Self-tuning closed-loop flux observer for sensorless torque control of standard induction machines," *IEEE Trans. Power Electron.*, vol. 12, pp. 807–815, Sept. 1997.

[12] H. Miyashita, Y. Fujita, and Ohmori, "Speed sensorless instantaneous vector control with identification of secondary resistance," in *Proc. Conf. Rec. IEEE-IAS Annu. Meeting*, 1991, pp. E130–E135.

[13] J. Jiang and J. Holtz, "High dynamic speed sensorless ac drive with on-line model parameter tuning for steady-state accuracy," *IEEE Trans. Ind. Electron.*, vol. 44, pp. 240–246, Apr. 1997.

[14] B. H. Kenny and R. D. Lorenz, "Stator and rotor flux based deadbeat direct torque control of induction machines ," in *Proc. Conf. Rec. 2001 IEEE 36th IAS Annu. Meeting*, vol. 1, pp. 133–9.

[15] M. Tursini, R. Petrella, and F. Parasiliti, "Adaptive sliding-mode observer for speed-sensorless control of induction motors," *IEEE Trans. Ind. Applicat.*, vol. 36, pp. 1380–1387, Sept./Oct. 2000.

[16] F. J. Lin, R. J. Wai, and P. C. Lin, "Robust speed sensorless induction motor drive," *IEEE Trans. Aerosp. Electron. Syst.*, vol. 35, pp. 566–578, Apr. 1999.

[17] Z. Yan, C. Jin, and V. I. Utkin, "Sensorless sliding_mode control of induction motors," *IEEE Trans. Ind. Electron.*, vol. 47, pp. 1286–1297, Dec. 2000.

[18] A. Derdiyok, H. Rehman, M. K. Guven, N. Inanc, and L. Xu, "A robust sliding mode observer for speed estimation of induction machine," in *Proc. Appl. Power Electron. Conf.*, vol. 1, 2001, pp. 413–418.

[19] G. R. Slemon, "Modeling of induction machines for electric drives," *IEEE Trans. Ind. Applicat.*, vol. 25, pp. 1126–1131, Nov./Dec. 1989.

[20] S. I. Moon, A. Keyhani, and S. Pillutla, "Nonlinear neural-network modeling of an induction machine," *IEEE Trans. Contr. Syst. Technol.*, vol. 7, pp. 203–211, Mar. 1999.

[21] P. Pillay, R. Nolan, and T. Haque, "Application of genetic algorithms to motor parameter determination for transient torque calculations," *IEEE Trans. Ind. Applicat.*, vol. 33, pp. 1273–1282, Sept./Oct. 1997.

[22] J. Stephan, M. Bodson, and J. Chiasson, "Real-time estimation of the parameters and fluxes of induction motors," *IEEE Trans. Ind. Applicat.*, vol. 30, pp. 746–759, May/June 1994.

[23] X. Xu and D. W. Novotny, "Implementation of direct stator flux orientation control on a versatile DSP based system," *IEEE Trans. Ind. Applicat.*, vol. 27, pp. 694–700, July/Aug. 1991.

[24] C. Wang, D. W. Novotny, and T. A. Lipo, "An automated rotor time constant measurement system for indirect field-oriented drives," *IEEE Trans. Ind. Applicat.*, vol. 24, pp. 151–159, Jan./Feb. 1988.

[25] S. Wade, M. W. Dunnigan, and B. W. Williams, "New method of rotor resistance estimation for vector-controlled induction machines," *IEEE Trans. Ind. Electron.*, vol. 44, pp. 247–257, Apr. 1997.

[26] R. Marino, S. Peresada, and P. Tomei, "On-line stator and rotor resistance estimation for induction motors," *IEEE Trans. Contr. Syst. Technol.*, vol. 8, pp. 570–579, May 2000.

[27] H. A. Toliyat, M. S. Arefeen, K. M. Rahman, and D. Figoli, "Rotor time constant updating scheme for a rotor flux-oriented induction motor drive," *IEEE Trans. Power Electron.*, vol. 14, pp. 850–857, Sept. 1999.

[28] M. Ehsani, K. M. Rahman, and H. A. Toliyat, "Propulsion system design of electric and hybrid vehicles," *IEEE Trans. Ind. Electron.*, vol. 44, pp. 19–27, Feb. 1997.

Amuliu Bogdan Proca (S'96) received the M.S.E.E. and Ph.D. degrees in electrical engineering from the Ohio State University, Columbus, OH, in 1997 and 2001, respectively.

He is currently working for Solidstate Controls Inc., Columbus, OH. Mr. Proca's research interests are in the areas of induction machine control, modeling, parameter estimation, and design.

Ali Keyhani (F'98) received the Ph.D. degree from Purdue University, West Lafayette, IN, in 1975.

Currently, he is a Professor of Electrical Engineering at the Ohio State University, Columbus, OH. From 1967 to 1969, he worked for Hewlett-Packard Co., Palo Alto, CA, on the computer-aided design of electronic transformers.

His research interest is in control and modeling, parameter estimation, failure detection of electric machines, transformers, and drive systems.

John M. Miller (F'99) received the Ph.D. degree from Michigan State University, East Lansing, MI, in 1983.

He was a member of the technical staff at Texas Instruments, Dallas, TX, from 1976 to 1980. He joined Ford Motor Company Research Laboratory in 1983 to work on electric vehicle programs and vehicle electrical system simulation. His interests range from the development of novel electromechanical components to the advancement of 42-V electrical distribution system for vehicles. He became an Adjunct Professor of Electrical Engineering at Michigan State University in 1998. He is the holder of 27 U.S. patents and has authored 37 publications on automotive electrical and electronic systems.

Dr. Miller was awarded Most Outstanding Paper Award at Convergence, the International Congress on Transportation Electronics, in 1998. He received best automotive paper award from IEEE Vehicular Technology Society in 1999. In 2000, Dr. Miller was awarded the IEEE Third Millennium Medal for his contributions to IEEE and Southeastern Michigan Section where he holds the office of Vice Chair. He is a member of the MIT/Industry Consortium on Advanced Automotive Electrical and Electronic Systems and Components, a past member of the steering committee, and of the Ford-MIT Alliance on 42-V architecture.